A Light Scattering Study of the Self-Assembly of Dendron Rod−Coil Molecules

B. J. de Gans and S. Wiegand*

Max Planck Institut für Polymerforschung, Ackermannweg 10, 55128, Mainz, Germany

E. R. Zubarev and S. I. Stupp

Department of Materials Science and Engineering, Department of Chemistry, Medical School, Northwestern University, Evanston, Illinois 60208

Received: March 26, 2002; In Final Form: July 14, 2002

Dendron rod−coil molecules are a novel supramolecular building block, comprising a dendritic unit, a rodlike unit, and a coil unit (*J. Am. Chem. Soc.* **2001**, *123*, 4105). It was proposed that in solution these molecules assemble into ribbonlike aggregates of high aspect ratio. We report here on the self-assembly of DRC-molecules in 2-propanol and ethyl acetate as studied with static and dynamic light scattering. In 2-propanol, aggregation occurs on a time scale of minutes. In ethyl acetate, aggregation proceeds more slowly until an equilibrium is reached. Static light scattering on 2-propanol-based samples reveals the presence of rodlike aggregates that grow with time. The static light scattering data of the ethyl acetate samples could be fitted to Kholodenko's expression for the form factor of a wormlike chain (*Macromolecules* **1993**, *26*, 4179), yielding a persistence length of 45 nm. Dynamic light scattering on ethyl acetate-based samples shows three modes. The dominant mode corresponds to translation of aggregates. Interactions between aggregates are shown to be negligible. The relaxation time spectrum was converted into a mass distribution, showing that only a fraction of the dendron rod−coil molecules aggregate to form the one-dimensional objects. This accounts for the observed low absolute scattering intensity of the solutions studied.

1. Introduction

Supramolecular chemistry studies the formation of polymolecular structures through noncovalent forces. In this area of chemistry it is of interest to understand the basic principles that drive molecular self-assembly. The long term goal is to learn how to construct increasingly complex systems that have a hierarchical structure from nano- to macroscopic scales. Nature is of course a source of inspiration for this field. Advances in supramolecular chemistry can help us to understand biology and increase the sophistication of materials, devices, and pharmaceuticals.

Recently, a novel supramolecular building block was synthesized,[1] which consists of three units, a coil segment (an isoprene oligomer), a rodlike unit (a *p*-biphenylyl ester trimer), and a dendritic unit with functional groups. The molecular structure is shown in Figure 1A. Apart from the dendritic unit these "dendron rod−coils" (DRCs) are structurally similar to other "rod−coil" molecules reported recently.[2,3] Each of the units plays a different role in the process of structure formation. The dendritic units are capable of forming hydrogen bonds, whereas the *p*-biphenylyl ester units have a strong tendency to crystallize with $\pi-\pi$ stacked arrangements. On the other hand, the isoprene oligomers are coiled and therefore unable to crystallize. These coillike segments give rise to entropic repulsion as a third structure determining mechanism.

A structure for DRCs in solution was proposed,[1] on the basis of the XRD data of a model compound, consisting of the dendritic unit plus one *p*-biphenylyl unit. It is assumed that four DRC molecules form a cyclic tetramer via hydrogen bonds (see Figure 1B). The tetramers then form a columnar structure, with the individual tetramers stitched along the column axis via additional hydrogen bonds. In solid samples transmission electron microscopy (TEM) indeed revealed a network-like structure, consisting of 10 nm thick strands that can be microns in length. The height of the strands as measured with atomic force microscopy (AFM) is about 2 nm, so the strands observed can be described as ribbons.[1] All these methods provide only indirect evidence for the "true" structure in solution, and we therefore chose here both static and dynamic light scattering to learn about the in situ structure of the system as it forms in solvent.

The kinetics of self-assembly is strongly dependent on the choice of solvent. Initial experiments using 2-propanol as a solvent showed aggregation on a time scale of minutes. Therefore, 2-propanol is very well suited to study aggregate properties as a function of time, using an advanced multiangle static light scattering setup (see section 3.3). However, 2-propanol does not allow dynamic light scattering or more extensive static light scattering experiments, as in this case data collection times are of the order of hours. Further investigations showed that in ethyl acetate aggregation proceeds more slowly and that eventually a quasi-equilibrium state is reached. Therefore, ethyl acetate was our solvent of choice to study equilibrium properties.

The rest of the paper is organized as follows. Immediately hereafter a short introduction is given to static and dynamic light scattering, and the models we used to describe our data. Details with respect to sample preparation and experimental setup can be found in the Experimental Section, which is followed by a discussion of the results.

2. Theory

2.1. Static Light Scattering. Within the framework of the Rayleigh−Gans−Debye theory[4] the excess Rayleigh ratio $\Delta R(q)$

10.1021/jp025832t CCC: $22.00
Published on Web 08/30/2002

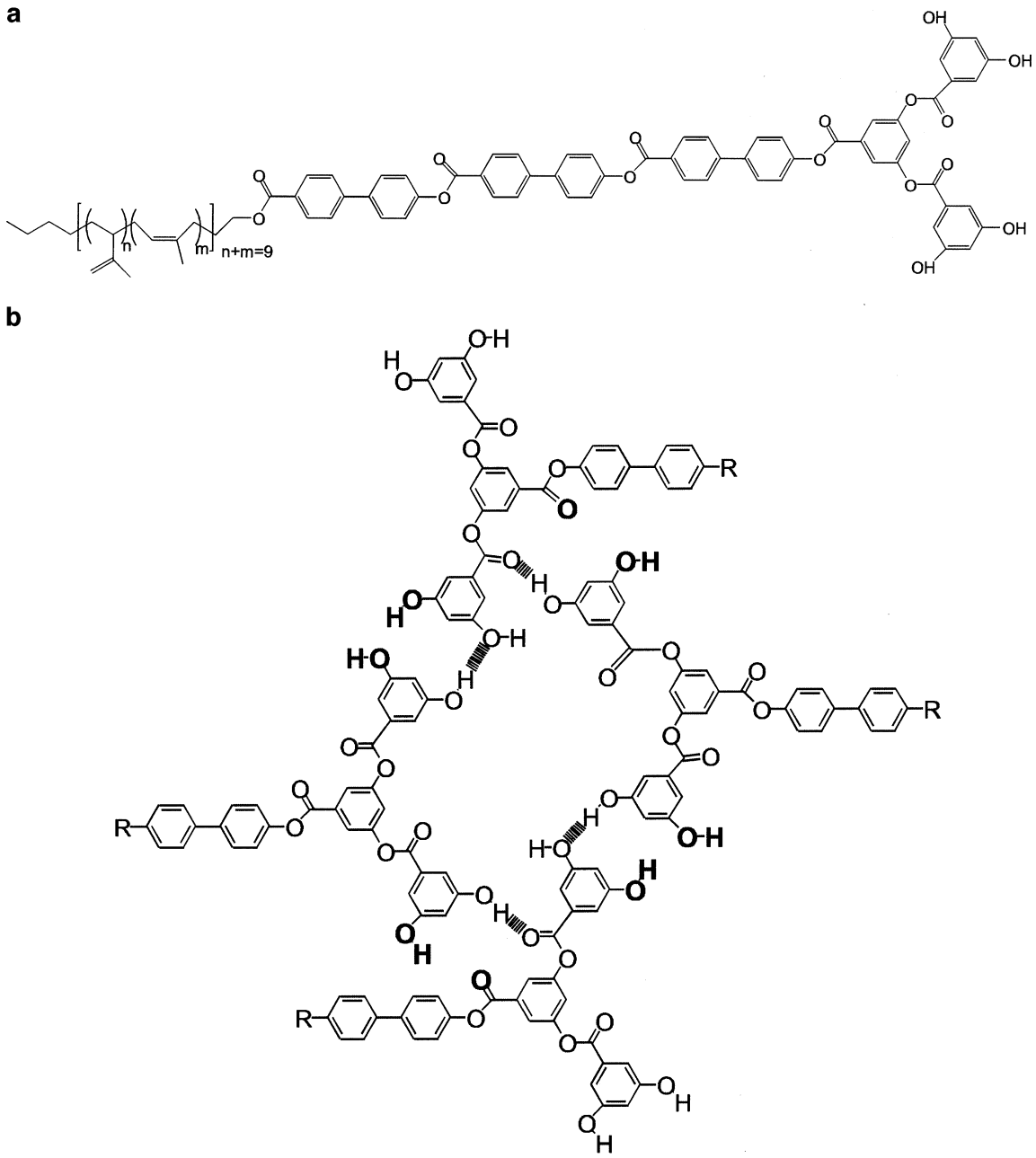

Figure 1. (A) Molecular structure of the dendron rod−coil molecule. (B) Sketch of four DRC molecules that form a cyclic tetramer via hydrogen bonds. These tetramers stack on top of each other, perpendicular to the plane of the paper, by additional hydrogen bonds that are formed by the bold marked hydroxyl and carbonyl groups.

can be written as

$$\Delta R(q) = KcM_w P(q)\, S(q) \tag{1}$$

where c is the concentration of the scattering objects, M_w is their weight-averaged molar mass, $P(q)$ is the form factor, and $S(q)$ is the structure factor. It will be shown later that for our system the contribution of the structure factor can be neglected; i.e., there is no interaction between the aggregates. The scattering vector $q = (4\pi^2 n_{solv}^2) \sin(\theta/2)/\lambda_0$, where θ denotes the measuring angle, λ_0 is the wavelength of the laser light in a vacuum, n_{solv} is the refractive index of the solvent, and K is the optical constant (see section 3.4).

The form factor of strongly anisometric DRC ribbons can be written as the product of an axial and a cross-sectional part,[5]

$$P(q) = P_{axial}(q) e^{-(1/2)q^2 R_{G,cs}^2} \tag{2}$$

We estimate the cross-sectional radius of gyration $R_{G,cs}$ of a 10 nm ribbon to be 3 nm. The maximum scattering vector accessible in our experiment is 0.025 nm^{-1}. It follows that the cross-sectional part of the form factor accounts for a 0.1% decrease of the scattering intensity only and may therefore be neglected. This implies that an important feature of the structure that was proposed for DRCs in solution, i.e., a ribbonlike cross-section, cannot be checked using light scattering.

The simplest model that may be used to describe the axial part is that of a rigid rod,

$$P_{rod}(q) = \frac{2}{qL}\int_0^{qL} \frac{\sin t}{t}\, dt - \frac{4 \sin^2(qL/2)}{q^2 L^2} \tag{3}$$

where L denotes the rod length. With increasing aggregate size, aggregate flexibility may come into play. A model that is often used to describe semiflexible chains is the wormlike chain,

characterized by chain length L_c and persistence length l_p. Approximate form factors for wormlike chains were recently compared by Pötschke et al.[6] The theory of Kholodenko[7] gave a good description of their Monte Carlo data. This theory gives the following expression for the form factor,

$$P_{\text{Kholodenko}}(q) = \frac{2}{x}\left[I_1(q,x) - \frac{1}{x}I_2(q,x)\right]$$

$$I_n(x,q) = \int_0^x \mathrm{d}z\, z^{n-1} f(z,q) \tag{4}$$

where $x = 3L_c/2l_p$. The function $f(z,q)$ is given by

$$f(z) = \begin{cases} \dfrac{\sinh(Ez)}{E\sinh(z)} & q \le \dfrac{3}{2l_p} \\ \dfrac{\sin(\hat{E}z)}{\hat{E}\sin(z)} & q > \dfrac{3}{2l_p} \end{cases} \tag{5}$$

and

$$E = \sqrt{1 - \left(\frac{2l_p q}{3}\right)^2} \qquad \hat{E} = \sqrt{\left(\frac{2l_p q}{3}\right)^2 - 1} \tag{6}$$

The theory of Kholodenko also gives an expression for the radius of gyration R_G of a wormlike chain,

$$R_G{}^2 = \frac{4l_p{}^2}{3x}\left[K_1(x) - \frac{1}{x}K_2(x)\right]$$

$$K_n(x) = \int_0^x \mathrm{d}z\, z^n\left(\coth z - \frac{1}{z}\right) \tag{7}$$

2.2. Dynamic Light Scattering. In a dynamic light scattering experiments the (normalized) intensity autocorrelation function $g_I(t)$ is measured, which is related to the field autocorrelation function $g_E(t)$ by the Siegert relation,

$$g_I(t) = 1 + g_E{}^2(t) \tag{8}$$

For the case of purely translational motion,

$$g_E = \mathrm{e}^{-t/\tau} \qquad \frac{1}{\tau} = q^2 D \tag{9}$$

where τ is the relaxation time and D the diffusion coefficient. From D a hydrodynamic radius R_H is calculated using the Stokes−Einstein relation,

$$D_{\text{sphere}} = \frac{k_b T}{6\pi\eta R_H} \tag{10}$$

which holds for noninteracting spheres. T denotes the temperature and η the vicosity of the solvent. Expressions do exist for the diffusion coefficient of wormlike chains,[9,11,13] but in this paper we will restrict ourselves to the determination of "equivalent" hydrodynamic radii, that is, the hydrodynamic radius that our aggregates would have had if they were spherical.

In the case of polydisperse systems a relaxation time distribution $G(\ln\tau)$ must be used,

$$g_E(t) = \int_{\ln\tau_{\min}}^{\ln\tau_{\max}} G(\ln\tau)\mathrm{e}^{-t/\tau}\,\mathrm{d}\ln\tau \tag{11}$$

which is obtained from $g_E(t)$ by CONTIN analysis.[14]

3. Experimental Section

3.1. Sample Preparation. Solutions of DRC in 2-propanol (Riedel-de Haën, p.A.) were prepared, containing 0.15% DRC by weight. Solutions were prepared in calibrated 5 mL flasks, which had been rinsed repeatedly with tetrahydrofuran and dried carefully before use at 50 °C. As DRC does not readily dissolve in 2-propanol, samples in carefully sealed flasks were heated in a boiling water bath for 30 s, then shaken manually, allowed to cool, and filtered through a 0.45 μm PTFE filter (Millipore). Cylindrical quartz cuvettes with a diameter of 20 mm (Hellma) were used as sample cells. All cuvettes were made dustfree by rinsing them with freshly distilled acetone for at least 15 min using an acetone fountain. Samples were measured immediately after preparation.

Solutions of DRC in ethyl acetate (Janssen Chimica, HPLC grade) were prepared having mass fractions of 0.0232, 0.0570, 0.115, and 0.227% by wt. Three solutions of each concentration were prepared in calibrated 5 mL flasks. Samples were shaken manually for 60 s, ultrasonicated for 120 s, again shaken manually for 60 s, and then filtered using a 0.2 μm PTFE filter (Millipore). As sample cells the previously mentioned cylindrical quartz cuvettes were used. Samples were stored for 2 months to ensure complete equilibrium, under ethyl acetate atmosphere to prevent evaporation of the solvent.

To check whether filtering results in loss of DRC the UV spectrum of a freshly prepared sample of DRC in ethyl acetate was measured in the range 300−400 nm, before and after filtering through a 0.2 μm Millipore filter. A Perkin-Elmer Lambda 2 instrument and rectangular quartz cuvette with a path length of 10 mm (Hellma) were used. No difference between the filtered and the unfiltered solution could be detected.

3.2. Dynamic Light Scattering. Dynamic light scattering measurements were carried out using an ALV 5000E instrument. All measurements were performed at room temperature using a krypton laser (Spectra Physics) of wavelength λ_0 in a vacuum equal to 647.1 nm. Its output varied between 50 and 250 mW depending on scattering strength. Correlation functions were measured in steps of 10° in the range 20−150°. Every angle was measured for 600 s to obtain a smooth correlation function. It was found that the samples with the lowest concentration of DRC, that is, 0.0232% by wt, lacked dynamical contrast, which impeded measurements at large angles. Therefore, for these samples measurements were only obtained in the range 20−70°. Correlation functions were analyzed using CONTIN.[14] Best solutions were chosen with a smoothing constraint $\alpha = 0.5$.

3.3. Static Light Scattering. Measurements were carried out using the instrument described previously. Data were taken every 3° ranging from 20° to 150°, and every angle was measured for 30 s. Data were corrected for solvent background and converted into Rayleigh ratios as follows,

$$\Delta R = \frac{I_{\text{solution}} - I_{\text{solv}}}{I_{\text{tol}}}\left(\frac{n_{\text{solv}}}{n_{\text{tol}}}\right)^2 R_{\text{tol}} \tag{12}$$

where I_{solution} and I_{tol} denote the scattered intensities corresponding to solution and toluene reference, respectively. n_{solv} and n_{tol} denote the refractive index of solvent and toluene. The Rayleigh ratio of toluene was taken to be 1.27×10^{-5} cm^{-1}.[10]

For the experiments on 2-propanol-based samples a home-built multiangle static light scattering setup was used.[11] The setup allows detection of the scattered intensity at 19 angles simultaneously, ranging from 26° to 143°. All measurements were performed at room temperature using a 647.1 nm krypton laser (Spectra Physics) at 100 mW output. Data were collected over 1000 runs, which corresponds to about 6 s. The advantage of the multiangle instrument as compared to the ALV setup lies in the speed of data acquisition, and the robustness of the

instrument; nonetheless, this instrument has less accuracy that the ALV 5000E.

3.4. Refractive Index Increment Determination. Refractive index increments for the calculation of the optical constant were measured at room temperature using a home-built setup,[12] operating at 633 nm. Ethyl acetate samples for refractive index increment determination were prepared as described previously but were left unfiltered and were stored for 1 day before measurement. It was found that $(\partial n/\partial c)_T = 0.217$ mL·g^{-1}. The optical constant K, defined as $K = 4\pi^2 n_{solv}^2 (\partial n/\partial c)_T^2/(N_{av}\lambda_0^4)$, was calculated as 3.32×10^{-11} mol·m^2·g^{-2}, where N_{av} is Avogadro's number.

4. Results and Discussion

4.1. Sample Preparation. The self-assembling behavior of molecules into supramolecular entities from solution is of course influenced by the nature of the solvent. Results described in ref 1 involved nanoribbons formed in dichloromethane and styrene. However, for the measurements described here we needed a solvent that would allow preparation of the sample (i.e., filtration of the sample) before substantial aggregation has taken place. It was found that ethyl acetate filfulled these conditions. Solutions could easily be filtered, as structure formation was found to occur on the time scale of hours. The prepared samples where completely clear and remained so during storage. Formation of a gel as described in ref 1 was not observed. On the contrary, in 2-propanol aggregation takes place on a time scale of minutes, and it is questionable whether samples can be prepared before aggregation starts. Therefore, filters with a larger pore size were used (0.45 μm instead of 0.2 μm) to prevent DRC losses during filtering. The samples could indeed easily be filtered. Immediately after preparation samples were completely clear. However, within 1 or 2 days after preparation a white precipitate was formed.

We found that the reproducibility of measurements improved when a stable solvent batch was used, that is, solvent stored for more than 1 year. This may be caused by the gradual dissolution of water from the air, as water is capable of forming hydrogen bonds and may therefore influence the formation of ribbons.

4.2. 2-Propanol-Based Samples. Figure 2A shows the scattering curve as a function of time of a sample that contained 0.149% DRC by weight. The solid lines are fits to the data according to eq 3. It is seen that the model fits the data very well. The rod length increases with time, as shown in Figure 2B.

From the scattering curves the radius of gyration R_G of the scattering objects can be obtained using the Guinier approximation,

$$\lim_{q\to 0} \Delta R(q) \sim e^{-(1/3)q^2 R_G} \qquad (13)$$

Interactions between aggregates are assumed negligible. No assumption is being made with repect to the shape of the objects. R_G is found by plotting ln ΔR versus q^2 and fitting a third-order polynomial to the data. For rods, the radius of gyration is related to the rod length via $R_G = L/\sqrt{12}$. These calculated rod lengths are also shown in Figure 2B. The rod lengths obtained via form factor fits and those obtained via the radius of gyration agree within 2−3%. This is a strong indication that the right form factor was chosen to fit the data; i.e., the aggregates that are present in 2-propanol are truly rodlike.

4.3. Ethyl Acetate-Based Samples. *4.3.1. Dynamic Light Scattering.* Figure 3A shows some field autocorrelation functions

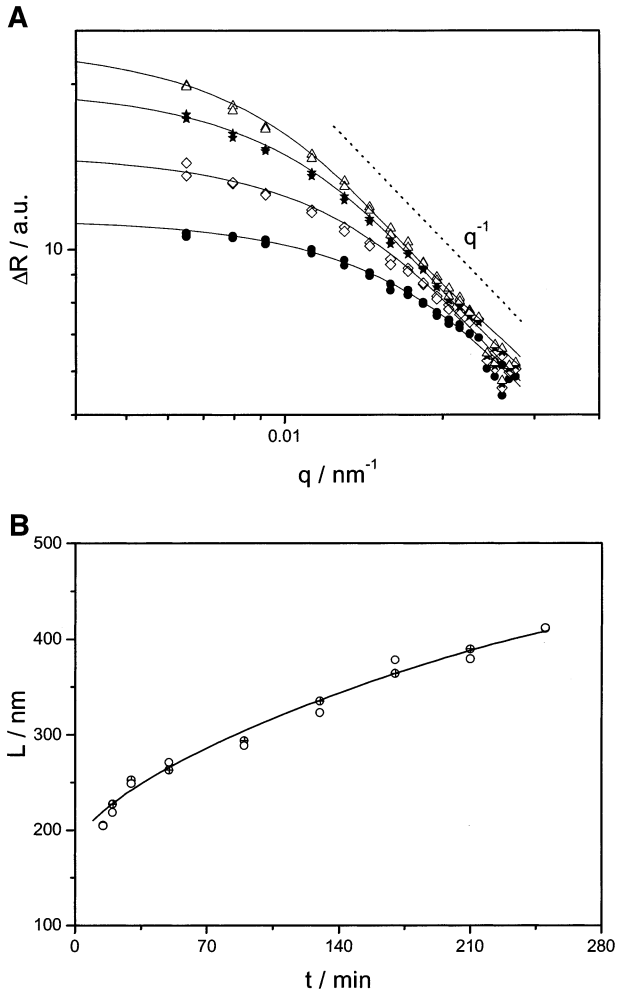

Figure 2. (A) Reduced excess scattering versus q of a 2-propanol-based sample, containing 0.149 wt % DRC. The solid lines are fits according to eq 3. Data were taken at different times after preparation: (●) 15 min; (◇) 50 min; (*) 130 min; (△) 210 min. The dotted line has slope −1, which is characteristic for rods at high q. (B) Fitted rod length and rod length calculated from the radius of gyration as a function of time: (⊕) fitted length; (○) calculated length. The line is drawn to guide the eye. The fitted and the calculated rod lengths agree remarkably well, usually within 2−3%.

obtained at different angles for a sample containing 0.115 wt % DRC. The corresponding (intensity weighted) relaxation time distributions resulting from CONTIN analysis are shown in Figure 3B. Autocorrelation functions and relaxation time distributions are representative for all concentrations. The CONTIN analysis reveals the presence of three relaxation processes. The average value of the dominant peak appearing in the relaxation time spectrum is plotted in the inset of Figure 4 as relaxation rate $\Gamma = \tau^{-1}$ versus q^2. Γ increases in approximately linear fashion with q^2, indicating translational diffusion. In Figure 4 the diffusion coefficient D was plotted as a function of q^2. Extrapolation to $q^2 \to 0$, using a linear or quadratic fit, gives the purely translational diffusion coefficient; i.e., internal modes do not contribute. The results of the extrapolation for different concentrations are listed in Table 1, together with the equivalent hydrodynamic radii R_H calculated using eq 10.

To check the assumption that (hydrodynamic) interactions between aggregates are negligible, we carried out the following experiment: A sample containing 0.114 wt % DRC was diluted stepwise up to 0.0220 wt % After each dilution step the equivalent hydrodynamic radius was measured at 60° and 90°.

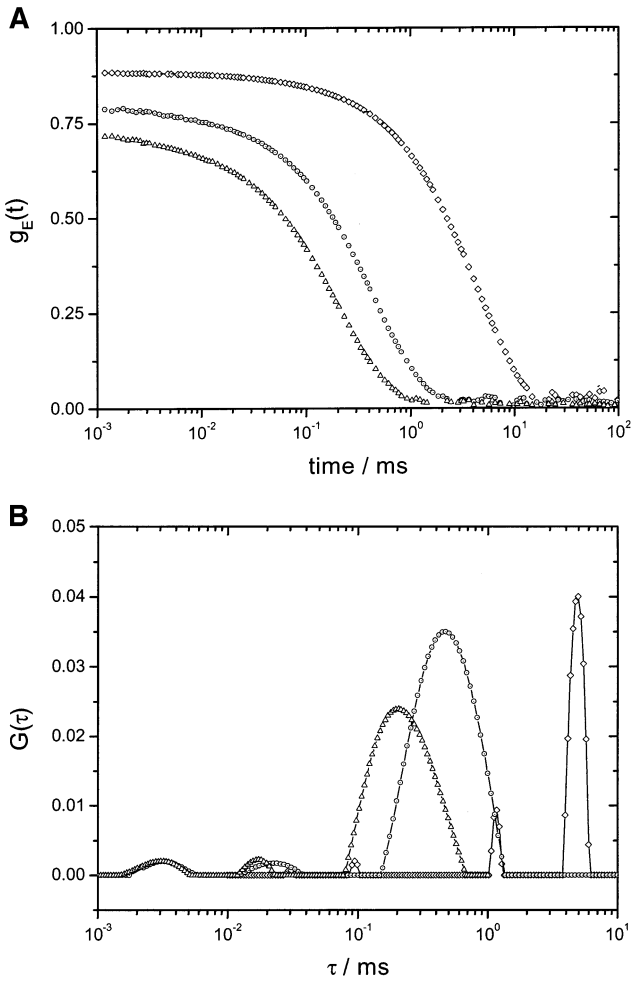

Figure 3. (A) Electric field autocorrelation functions $g_E(t)$ of an ethyl acetate-based sample, containing 0.115 wt % DRC: (◇) 30°; (⊙) 90°; (△) 150°. $\phi_m = 0.114$ wt %. (B) Relaxation time spectrum obtained from CONTIN analysis of electric field autocorrelation functions as shown in Figure 1: (◇) 30°; (⊙) 90°; (△) 150°. Every spectrum shows three peaks.

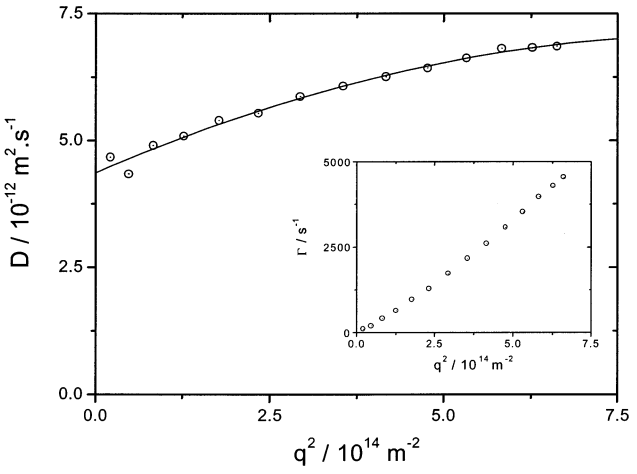

Figure 4. Diffusion constant D corresponding to the dominating mode in the relaxation time spectrum (see Figure 3B). The drawn line is a quadratic fit to the data. Mass fraction $\phi_m = 0.114$ wt %. The inset shows the corresponding relaxation rates. The approximately linear increase of Γ with q^2 indicates a translational process.

It was found that the hydrodynamic radius did not change within an error of 4% (60°) to 8% (90°), which means that interactions do not play a role.

TABLE 1: Diffusion Constants D of the Dominant Translational Mode in the Relaxation Time Spectrum, and Corresponding Hydrodynamic Radii R_H

ϕ_m/wt %	$D/10^{-12}$ m²•s^{-1}	R_H/nm
0.0232	11.1 ± 2.6	46 ± 11
0.0570	4.24 ± 0.2	114 ± 5
0.115	4.51 ± 0.1	107 ± 2
0.207	5.74 ± 0.2	84 ± 3

TABLE 2: Measured Radii of Gyration $R_{G,meas}$, and Chain Lengths L_c[a]

ϕ_m/wt %	c/g•L^{-1}	$R_{G,meas}$/nm	L_c/nm	$R_{G,calc}$/nm
0.0232	0.205	83 ± 8	496 ± 105	78 ± 10
0.0570	0.503	105 ± 3	1172 ± 16	128 ± 1
0.115	1.01	100 ± 2	773 ± 65	102 ± 5
0.207	2.01	88 ± 3	507 ± 13	80 ± 1

[a] In the last column the radii of gyration $R_{G,calc}$ are listed that were calculated using eq 7, assuming a persistence length $l_p = 45$ nm.

The interpretation of the two small peaks in the relaxation time spectra is very difficult. They correspond to less than 10% of the total scattered intensity and their behavior as a function of q is poorly reproducible. The first peak usually appears at $R_H = 1.0-1.5$ nm and may therefore account for the presence of monomers or tetramers of dendron rod−coil molecules. Tetramers were previously suggested as the monomeric units forming ribbons.[1] However, given the quality of the data, any attempt to interpret them remains speculative.

4.3.2. Static Light Scattering. Figure 5A shows the scattering curves of some samples. Figure 5B shows Guinier plots of the same data as in Figure 5A, i.e., ln ΔR plotted versus q^2. The drawn lines are quadratic fits to the data. Thus obtained radii of gyration are listed in Table 2. More information can be obtained from the scattering curves when the data are plotted in a Holtzer-diagram, that is, $q\Delta R$ versus $u \equiv qR_G$.[15] For large q the excess Rayleigh ratio of rods and wormlike chains scales as q^{-1}. The corresponding Holtzer plot shows a plateau for large q. Figure 5C shows a Holtzer plot of the data from Figure 5A. It is seen that at the lowest weight fraction (0.0232 wt %) the aggregates indeed seem to be rodlike. At higher concentrations the curves pass through a (shallow) maximum before leveling off. This indicates that the aggregates are flexible to some extent.[16] In the case of monodisperse aggregates this maximum should occur at $u = 1.4$,[17] corresponding to the vertical line in Figure 5C. With increasing polydispersity the maximum shifts to higher values of u. Figure 5C shows that the samples that contain 0.0568 and 0.114 wt % DRC have a maximum at (approximately) $u = 1.4$ and are therefore monodisperse.

The scattering curves were also analyzed with the theory of Kholodenko. It was found that eq 4 fitted very well to the data corresponding to the two highest concentrations (0.115 and 0.207 wt %). All data corresponding to these two concentrations were fitted with a single persistence length. This seems physically founded, as we may expect that although the lengths of the aggregates vary from sample to sample, the cross-sectional structure (which determines the chain stiffness and therefore the persistence length) should be the same for all. A persistence length $l_p = 45$ nm was obtained. This relatively high persistence length may be explained by the observation that the ribbons twist themselves into a helix.[1] It is interesting that the mechanical properties of the aggregates depend on the solvent, as aggregates in 2-propanol were found to be rodlike, without flexibility.

All data were then fitted with the obtained persistence length as a fixed parameter. Results of the fitting procedure can be

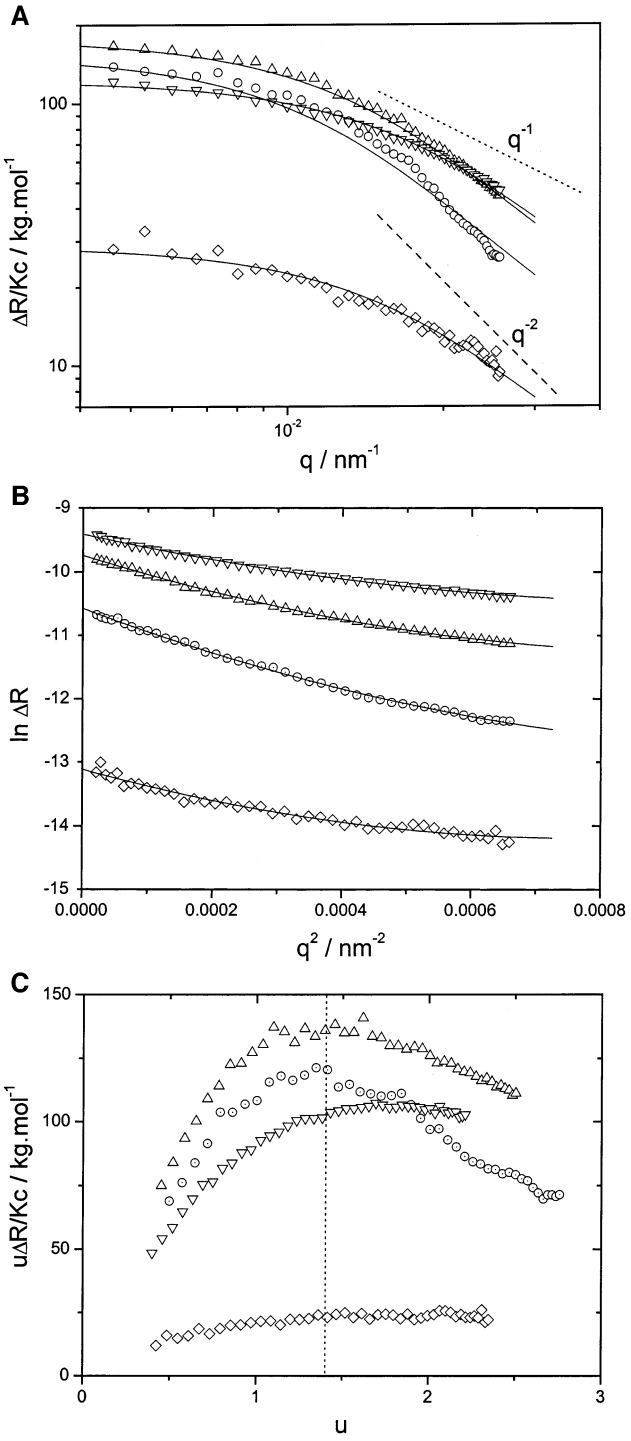

Figure 5. (A) Reduced excess scattering versus q for four different ethyl acetate-based samples: (◇) 0.0230 wt %; (⊙) 0.0568 wt %; (△) 0.114 wt %; (▽) 0.227 wt %. The drawn lines are fits according to eq 4. The dotted line has slope −1, which is characteristic for rods at high q. The dashed line has slope −2, which is characteristic for random coils. (B) Guinier representation of data from Figure 3A. The drawn lines represent quadratic fits to the data, from which the radius of gyration was determined, using that $\lim_{q\to 0} \ln \Delta R(q) = \ln \Delta R(0) - (1/3)q^2R_G^2 + O(q^4)$. (C) Holtzer representation of data from Figure 3A. $u \equiv qR_G$. The vertical line at $u = 1.4$ marks the position at which a maximum should appear if the sample were monodisperse. It can be seem that the samples ⊙ (0.0568 wt %) and △ (0.114 wt %) fulfill this condition.

seen in Figure 5A. The resulting chain lengths are listed in Table 2. To check the results, we calculated the radius of gyration using eq 7 and compared those to the experimentally obtained

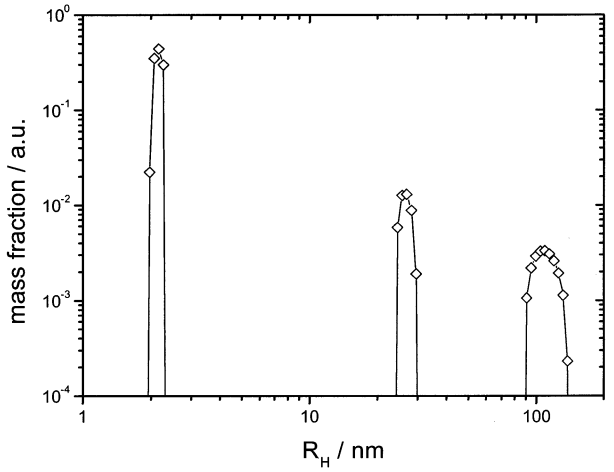

Figure 6. Distribution of mass fraction versus equivalent hydrodynamic radius R_H. It was assumed that $M_{part} \propto R_H^2$. Angle: 30°. $\phi_m = 0.114$ wt %. Monomers and tetramers account for the main part of the total mass of dendron rod−coils. Only a minor fraction has aggregated.

values. It was found that the agreement between both radii is reasonable, except for the samples containing 0.057 wt % DRC, where there is a significant difference.

To cross-check the results of the Kholodenko theory we tried to fit our data to the numerical expressions of Pedersen and Schurtenberger,[8] which according to Pötschke,[6] provide an even better description of the form factor of a wormlike chain. However, unphysically small values for the persistence length were obtained. It should be noted that the reproduced expressions in ref 6 contain errors. The correct expressions can be found in ref 8.

From the absolute scattering intensity at zero wave vector the molecular weight of the aggregate can be calculated, using eq 1. From Figure 5A it can immediately be seen that these are of the order of 100 000−200 000. A rough estimate of the molecular weight can also be obtained using the fitted chain lengths in Table 2. The molecular weight of a single dendron rod−coil is 1712. The distance between the tetramers that are supposed to make up the ribbon is 4.93 Å.[1] With 400 nm as a representative length, it follows that the molecular weights calculated from the absolute scattering intensity are more than an order of magnitude too small. Interactions cannot explain this effect, as DLS showed them to be negligible.

Another explanation for the loss of scattering power could be that these dendron rod−coil molecules aggregate only partially. If this is correct, to obtain an estimate of the molar mass using eq 1, one should only use for the concentration the fraction of molecules that has aggregated. Therefore the intensity weighted relaxation time spectrum from Figure 3B was converted to a mass distribution as a function of R_H. We can do this conversion because the intensity of light scattered by a particle $I \propto M_{part}^2$, where M_{part} denotes the particle mass and $M_{part} \propto R_H^{\alpha}$ (α varies between 1 for thin rods and 3 for spheres). We used a value of $\alpha = 2$, which corresponds to a Gaussian coil. The result is shown in Figure 6. It is seen that although monomers and tetramers account only for a few percent of the total scattering, they account for nearly all the mass. This implies that dendron rod−coils in ethyl acetate show a very weak tendency to aggregate.

5. Conclusions

Dendron rod−coils are a novel supramolecular building block. They consist of a dendritic unit, capable of forming hydrogen

bonds, a rodlike unit, and a flexible coil unit. TEM and AFM indicate that dendron rod−coils in solution spontaneously form a ribbonlike superstructure.[1] We investigated the in situ structure of DRC molecules as it forms in solution as a function of concentration using dynamic and static light scattering, and using 2-propanol and ethyl acetate as solvents. In 2-propanol structure formation takes place on a time scale of minutes. In ethyl acetate structure formation takes place on a time scale of hours to days.

The scattering curves of the 2-propanol-based samples can be fitted very well to the form factor of a rigid rod. The rod length increases with time, and agrees within a few percent with the rod length that was calculated from the radius of gyration.

A Holtzer plot of the scattering curves of the ethyl acetate-based samples showed the presence of aggregates with a high aspect ratio, which are flexible to some extent. A fit to the data using the expression of Kholodenko for the form factor of a wormlike chain yielded a persistence length $l_p = 45$ nm and a concentration dependent chain length. From the persistence length and the chain length the radius of gyration was calculated. It agrees well with the measured radius of gyration. Details with respect to the cross-sectional structure of the aggregates cannot be revealed using light scattering.

The relaxation time spectrum, obtained by CONTIN analysis of the field autocorrelation function shows the presence of three peaks. The dominant peak corresponds to the translation of aggregates. The diffusion coefficient was obtained in the hydrodynamic limit, from which the equivalent hydrodynamic radius was calculated. The hydrodynamic radius did not change after dilution of the sample; i.e., the aggregates do not interact.

The absolute scattering intensity of the ethyl acetate-based samples is too low to account for aggregates of the size found. By conversion of the relaxation time spectrum to a mass distribution, it was shown that the small peaks in the relaxation time spectrum account for the major part of total mass, implying that only a small fraction of the dendron rod−coils in ethyl acetate have actually aggregated.

Acknowledgment. P. Räder is thanked for performing the Karl Fischer titration.

References and Notes

(1) Zubarev, E. R.; Pralle, M. U.; Sone, E. D.; Stupp, S. I. *J. Am. Chem. Soc.* **2001**, *123*, 4105−4106.
(2) Stupp, S. I.; LeBonheur, V.; Walker, K.; Li, L.; Huggins, K. E.; Keser, M.; Amstutz, A. *Science* **1997**, *276*, 384−389.
(3) Pralle, M. U.; Whitaker, C. M.; Brown, P. V.; Stupp, S. I. *Macromolecules* **2000**, *33*, 3550−3556.
(4) Dhont, J. K. G. *An Introduction to Dynamics of Colloids*; Elsevier: Amsterdam, 1996; p 109.
(5) Porod, G. In *Small-Angle X-ray Scattering*; Glatter, O., Kratky, O., Eds.; Academic Press: London, 1982; p 32.
(6) Pötschke, D.; Hickl, P.; Ballauff, M.; Åstrand, P. O.; Pedersen, J. S. *Macromol. Theory Simul.* **2000**, *9*, 345−353.
(7) Kholodenko, A. L. *Macromolecules* **1993**, *26*, 4179−4183.
(8) Pedersen, J. S.; Schurtenberger, P. *Macromolecules* **1996**, *29*, 7602−7612.
(9) Benoit, H.; Doty, P. *J. Phys. Chem.* **1953**, *57*, 958.
(10) Schmidt, M. Private communication.
(11) Becker, A.; Schmidt, M. *Makromol. Chem., Macromol. Symp.* **1991** *50*, 249−260.
(12) Becker, A.; Köhler, W.; Müller, B. *Ber. Bunsen-Ges. Phys. Chem.* **1995**, *99*, 600−608.
(13) Harnau, L.; Winkler, R. G.; Reineker, P. *J. Chem. Phys.* **1996** *16*, 6355−6368.
(14) Provencher, S. *Comput. Phys. Commun.* **1982**, *27*, 213−239.
(15) Holtzer, A. *J. Polym. Sci.* **1955**, *17*, 432−434.
(16) Schmidt, M.; Paradossi, G.; Burchard, W. *Makromol. Chem., Rapid Commun.* **1985**, *6*, 767−772.
(17) Denkinger, P.; Burchard, W. *J. Polym. Sci., Part B: Polym. Phys.* **1991**, *29*, 589−600.